Journal of Applied Electrochemistry (2006) 36:669–676
DOI 10.1007/s10800-006-9119-x

Effects of current density on the structure of Ni and Ni–Mn electrodeposits

E. A. MARQUIS[1,*], A. A. TALIN[1], J. J. KELLY[1,3], S. H. GOODS[1] and J. R. MICHAEL[2]
[1]*Sandia National Laboratories, 7011 East Avenue, Livermore, CA 94550, USA*
[2]*Sandia National Laboratories, Albuquerque, NM 87185, USA*
[3]*IBM/ T.J. Watson Research Center, Yorktown Heights, NY 10598, USA*
*(*author for correspondence, tel.: + 1-925-294-3287, fax: + 1-925-294-3231, e-mail: emarqui@sandia.gov)*

Received 21 July 2005; accepted in revised form 6 January 2006

Key words: atom probe tomography, electrodeposition, microstructure, Ni, Ni–Mn, sulfamate bath, texture

Abstract

Grain size and texture of Ni electrodeposited from sulfamate baths depend greatly on current density. Increasing grain size is observed with increasing current density and the deposit texture changes from ⟨110⟩ at current densities lower than 5 mA cm^{-2} to ⟨100⟩ for higher current densities. Co-deposition of Mn modifies the deposit structure by favoring the growth of the ⟨110⟩ texture and decreasing the average grain size even as the current density increases. While the average Mn film content increases with increasing current density, local Mn concentrations are a more complex function of deposition parameters, as indicated by atom probe tomography measurements. In both direct-current plated and pulse plated films, large variations on a nanometer scale in local Mn concentration are observed.

1. Introduction

The combination of high mechanical strength with thermal stability and low residual stress in electrodeposited (ED) Ni is highly desirable for many applications, though rarely achievable in practice. High strength and hardness generally require extremely fine grain sizes, which in turn lead to greater driving force for recrystallization and grain growth, and therefore, decreased thermal stability. Thus, nanocrystalline ED Ni with yield strength of ~1.5 GPa begins to recrystallize at temperatures as low as 100 °C [1]. Previous work has shown that incorporation of Mn into ED Ni significantly increases yield strength and improves thermal stability [2]. ED Mn-free Ni has a typical yield strength range of 300–600 MPa and loses 60% of its as deposited strength after a 1 h anneal at 400 °C [3]. ED Ni–Mn, however, has a yield strength range of of 800–1100 MPa, and retains 80% of its strength even after 1 h anneal at 600 °C [4]. Addition of Mn, however, also dramatically increases the residual stress, thereby limiting the thickness of the plated films. Recently, a high strength, low residual stress Ni–Mn alloy with Mn concentration of ~0.4 at.% has been developed primarily for high aspect ratio microsystem applications [2]. In order to limit the film stresses accumulated during deposition, pulse-plating conditions are used with the hypothesis that they create a material that is compositionally modulated at the nanoscale [5, 6]. The resulting material is believed to consist of regions of high-stress Ni–Mn separated by regions of low-stress Ni, but the distribution of Mn has never been experimentally observed and the compositional structure remains hypothetical.

Understanding of the thermal stability of ED Ni–Mn requires accurate description of the as-deposited structure, and in particular the effects of the deposition parameters in order to compare the behavior of ED Ni and ED Ni–Mn. Ni sulfamate baths are attractive for electroforming and other applications that require thick deposits as they produce low stress, high ductility and higher purity Ni deposits than Watts baths, which are predominantly used for decorative and protective Ni coating [7]. For most ED metals, the texture is independent of the substrate for films thicker than several microns, and is rather controlled by pH, current density, and presence of organic additives. In the case of Watts Ni, two general growth regimes have been defined [8]: a regime of ''free'' growth where the films develop a strong ⟨100⟩ texture, and a regime of ''inhibited'' growth dominated by other orientations, including ⟨110⟩, ⟨211⟩, or ⟨210⟩. Hydrogen adsorption on the growing Ni surface is considered as one leading inhibition mechanism [8]. Unlike Watts Ni, the texture and microstructure of Ni sulfamate as a function of current density, pH, and bath additives have not been extensively investigated.

The present paper focuses on the effects of current density and the presence of $MnCl_2$ in the electrolyte on the texture and microstructure of Ni ED. Analyses of

the mechanisms responsible for the thermal stability will be presented elsewhere [9].

2. Experimental

2.1. *Electrodeposition*

A detailed description of the electrodeposition method used here is published elsewhere [2]. The deposition parameters used to fabricate the sulfamate Ni and Ni–Mn materials at constant current density (DC) are summarized in Table 1. Pulse plated (PP) Ni–Mn materials were produced with a square waveform from the same electrolyte with added $MnCl_2{\cdot}4H_2O$. In the first step of the pulse plating waveform, a current density i_1 of 3 mA cm^{-2} was applied for $t_1 = 4.4$ s, while for the second step $i_2 = 15$ mA cm^{-2} and $t_2 = 0.667$ s.

Blanket films with a thickness of 5–10 μm plated on polished copper substrates were used to characterize the grain structure and texture of the Ni and Ni–Mn materials while thicker deposits (200–300 μm) were fabricated for transmission electron microscopy (TEM) observations. After plating, these thicker specimens were freed from the underlying Cu by selective chemical dissolution of the Cu.

2.2. *Characterization*

Specimen texture was determined using a Philips X'Pert MRD X-ray diffractometer with a Cu anode operated at 45 kV and 40 mA. Pole figures corresponding to (111), (200), and (220) reflections were collected for azimuthal rotation of $0 \le \phi \le 360°$ and tilt angle of $0 \le \psi \le 90°$ in 5° increments. The experimental pole figures were corrected for absorption and defocusing using a Ni powder specimen [10]. Based on the experimental pole figures (data only for $\psi \le 80°$ was used), orientation distribution functions (ODFs) were computed using the BEARTEX program [11]; the ODFs were in turn used for calculation of inverse pole figures. Mn concentration was measured using a Kevex X-ray fluorescence spectrometer with a Mo/Nb anode set at 50 kV and a source aperture of 50 μm.

A FEI DB235 dual beam focused ion beam scanning electron microscope (FIB-SEM) was used to characterize the grain morphology of as-deposited films in cross-section employing the ion beam-induced channeling contrast imaging capabilities of the FIB instrument [12]. The depth of penetration of the ions is related to the crystallographic orientation of individual grains. As such, certain crystallographic orientations result in stronger ion channeling and therefore deeper penetration of the ions into the sample. Deeper ion penetration, in turn, produces fewer collectable secondary electrons, so strongly channeling orientations appear dark as compared to more weakly channeling orientations. The amount of channeling is quite sensitive to small variations (1–2°) in orientation so that not only can grains of different orientations be imaged, but small misorientations within a grain are visualized as well.

In-plane TEM samples were prepared by electropolishing 3-mm discs using a solution of 10% perchloric acid in methanol at −30 °C. TEM was performed using a JEOL 2010F microscope operated at 200 kV.

Atom probe tomography (APT) specimens were prepared in the form of sharp needles oriented so that their axis was either parallel to the plating direction (out-of-plane tip) or perpendicular to the plating direction (in-plane tip) (Figure 1). The out-of-plane tips were prepared using precision dicing techniques to form small posts with a cross-section of about 20×20 μm^2, that were thinned to the shape of a sharp needle using a gallium focused ion beam. The in-plane tips were prepared using standard electropolishing procedures [13]. APT analyses were performed using a LEAP microscope (Imago Scientific Instruments). The tips were held at relatively high temperatures (between 60 and 80 K) during field ion evaporation to limit the electric field applied on the tips, which were prone to fracture due to the small grain size.

3. Results

3.1. *Texture*

The current density used for deposition of Ni sulfamate films influences the deposit texture. At low current densities (≤5 mA cm^{-2}), the ⟨110⟩ orientation along the plating direction dominates (Figure 2(a) and (c)). Higher current densities (≥10 mA cm^{-2}) favor the ⟨100⟩ direction along the plating direction (Figure 2(e) and

Table 1. Deposition parameters

Temperature	28 ± 1 °C
pH	3.5
Bath composition	1.35 M Ni-sulfamate 0.49 M boric acid 0.2 g l^{-1} sodium dodecyl sulfate For Mn deposition, addition of 0.091 M $MnCl_2{\cdot}4H_2O$
Current density	3–15 mA cm^{-2} (as indicated)

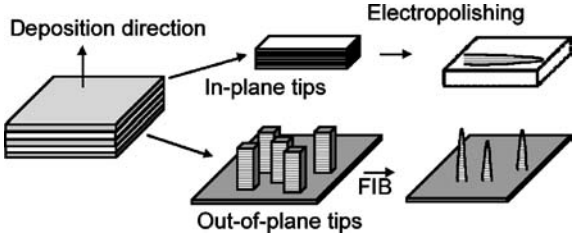

Fig. 1. Schematic of APT specimen preparation.

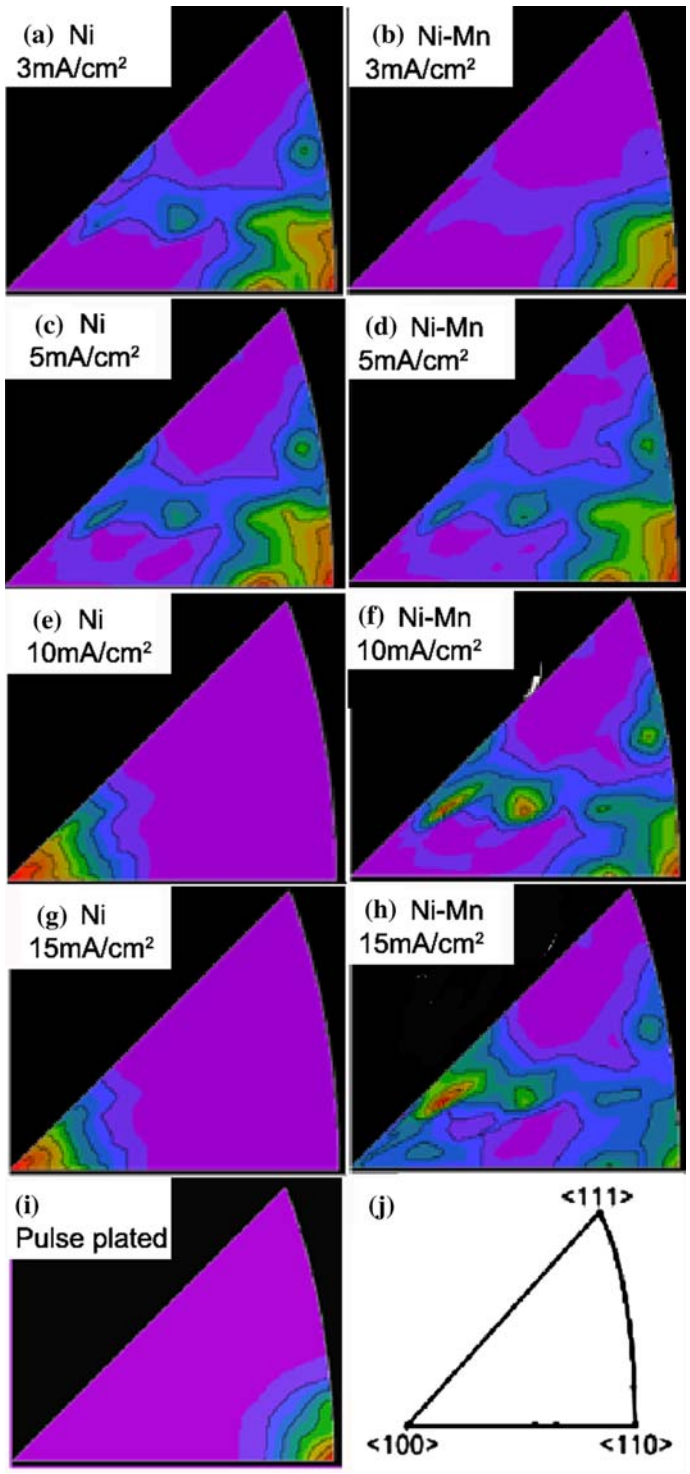

Fig. 2. Texture (inverse pole figures) of Ni and Ni–Mn deposits as a function of current density. (a,b) correspond to Ni and DC Ni–Mn, respectively, deposited at 3 mA cm^{-2}; (c,d) 5 mA cm^{-2}; (e,f) 10 mA cm^{-2}; (g,h) 15 mA cm^{-2}; and (i) illustrates the texture of PP Ni–Mn. For reference, (j) is a schematic IPF corresponding to a ⟨100⟩ equal area projection with indication the main orientations.

(g)). Mn addition does not affect the texture of Ni deposits at low current density. The ⟨110⟩ direction is still the dominant orientation along the plating direction for current densities ≤ 5 mA cm^{-2} (Figure 2(b) and (d)). Higher current densities used for deposition of Ni–Mn deposits, however, promote the appearance of higher index directions while maintaining the presence of grains with the ⟨110⟩ orientation along the plating direction (Figure 2(f) and (h)). Similarly to Ni and DC Ni–Mn plated at low current densities, pulse-plated Ni–Mn deposits exhibit a strong ⟨110⟩ texture as well (Figure 2(i)).

3.2. *Grain structure*

The current density during deposition of Ni from Ni sulfamate baths greatly influences its grain structure, as shown by the cross-sectional FIB-SEM images, where different grayscale shadings correspond to different grain orientation as described above (Figure 3). In these images, the blanket films are still attached to the copper substrates (with a cube texture), which appear as extremely coarse-grained regions at the bottom of each micrograph. The structure of the deposits at the Cu interface is initially equiaxed, but with continued growth, rapidly evolves into columnar morphologies characteristic of the bulk microstructure for all studied conditions. The effect of current density is most visible for pure Ni deposits. They exhibit significantly larger grain sizes as current density increases to and above 10 mA cm^{-2}. Figure 3(a)–(d) shows that many grain extend through a large fraction of the film thickness ($\sim$10 μm) of the deposits. In contrast to pure Ni, the grain structure of DC plated Ni–Mn deposits remains very fine for all current densities (Figure 3(e)–(h)).

Average grain sizes were obtained from TEM observations by line-intercept measurements. At low current densities ($\leq$5 mA cm^{-2}), the average in-plane grain size of Ni is 80 ± 27 nm. Higher current densities ($\geq$10 mA cm^{-2}) lead to coarser grain structure, and the in-plane grain size is significantly larger (290 ± 20 nm at 15 mA cm^{-2}). When plated at 3 mA cm^{-2}, the structure of DC plated Ni–Mn deposits is very comparable to that of Ni with an average grain size at 3 mA cm^{-2} of 93 ± 15 nm. High twin densities are observed in all plated films, and Figure 4 compares the grain structure as observed by TEM. The pulse-plated Ni–Mn films (Figure 4(c)) exhibit a finer grain structure (average in-plane size equal to 43 ± 7 nm), than that of DC-plated Ni (Figure 4(a)) and Ni–Mn (Figure 4(b)) both plated at 3 mA cm^{-2}.

3.3. *Mn distribution*

The incorporation of Mn increases with increasing current density. At 3 mA cm^{-2}, the Mn concentration is 0.12 at.% as measured from ICP-OES. X-ray-fluorescence

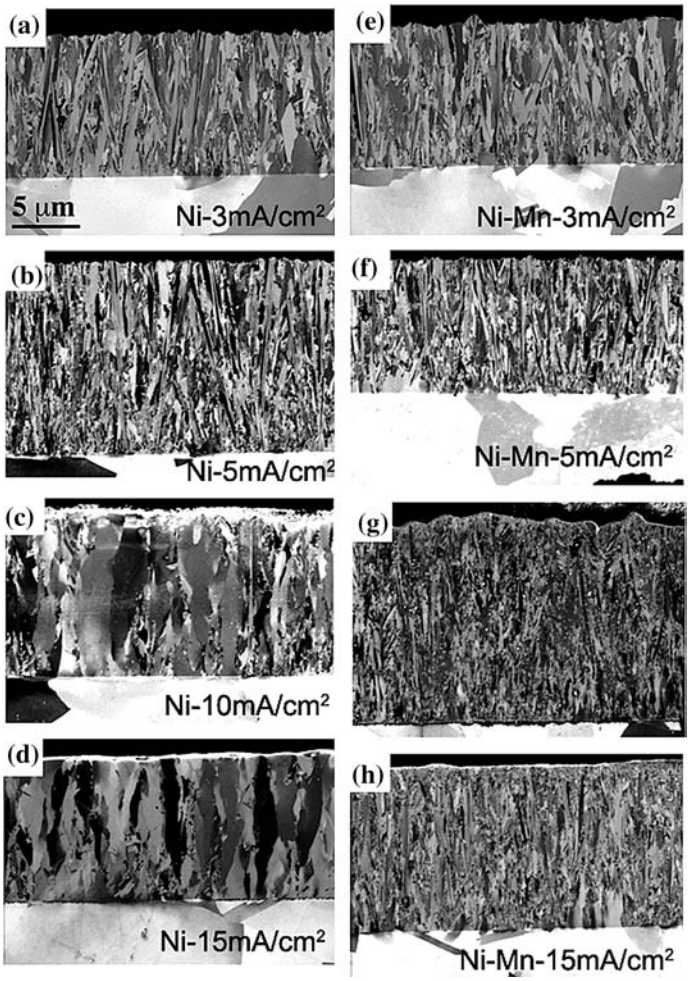

Fig. 3. FIB-SEM images of cross-sections from Ni and DC Ni–Mn deposits for different current densities: (a,e) correspond to Ni and Ni–Mn at 3 mA cm^{-2}, (b,f) 5 mA cm^{-2}, (d,g) 10 mA cm^{-2}, and (d,h) 15 mA cm^{-2}.

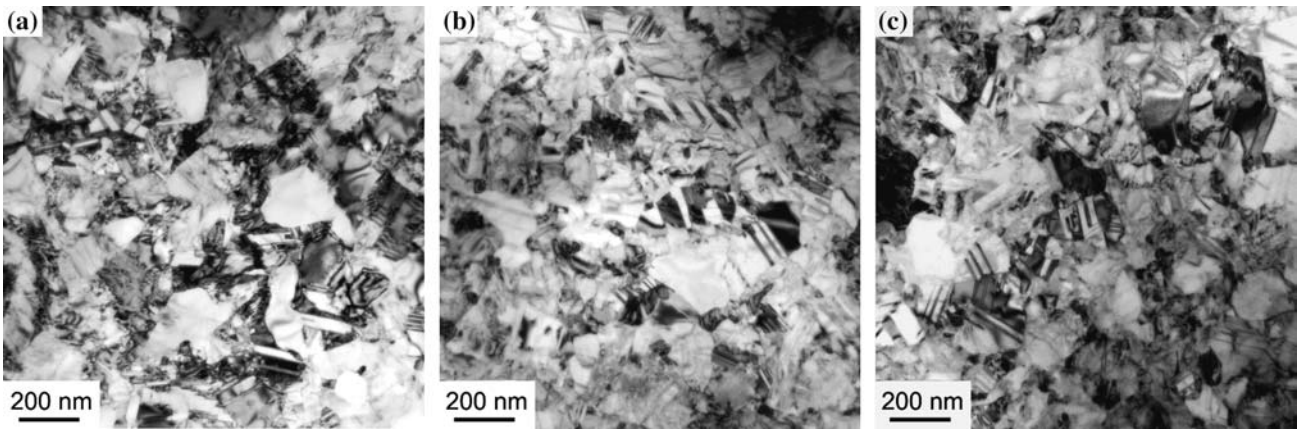

Fig. 4. TEM images of (a) Ni deposited at 3 mA cm^{-2}, (b) DC plated Ni–Mn deposited at 3 mA cm^{-2} and (c) PP Ni–Mn.

measurements for Ni–Mn specimens plated at 5, 10, and 15 mA cm^{-2}, yield concentrations of 0.29, 0.48, and 0.62 at.% Mn respectively, indicating a monotonic dependence of the Mn concentration with current density, as previously reported [4]. Since the overall deposit thickness depends approximately linearly on current density, integration of Faraday's law indicates that the pulse-plating process should result in Ni deposits with ~0.4 at.% Mn, as was confirmed by XRF measurements which yielded 0.40 ± 0.05 at.%.

When viewed via conventional electron microscopy (TEM or SEM), the defect microstructures (twins, grain boundaries, etc.) in Ni, DC plated Ni–Mn and PP Ni–Mn films do not yield any evidence suggesting a layered or compositionally modified material. APT results clearly indicate that the Mn distribution is non-uniform in PP and in DC plated Ni–Mn deposits. The topology of the Mn concentration varies from sample to sample; some samples exhibit a 'layered' structure, as intended through the pulse-plating process, whereas others present Mn concentrations that are modulated in all directions. For instance, in the case of PP Ni–Mn, a pattern was obtained from a tip in the out-of-plane geometry with layers at about 45° to the plating direction (Figure 5(a)). The concentration profile taken along the direction parallel to the plating direction show that the Mn concentration oscillates between 0 and 1.2 at.% with a spatial periodicity along the deposition direction of about 10 nm. Another analysis of an in-plane tip also indicates layering with a spatial

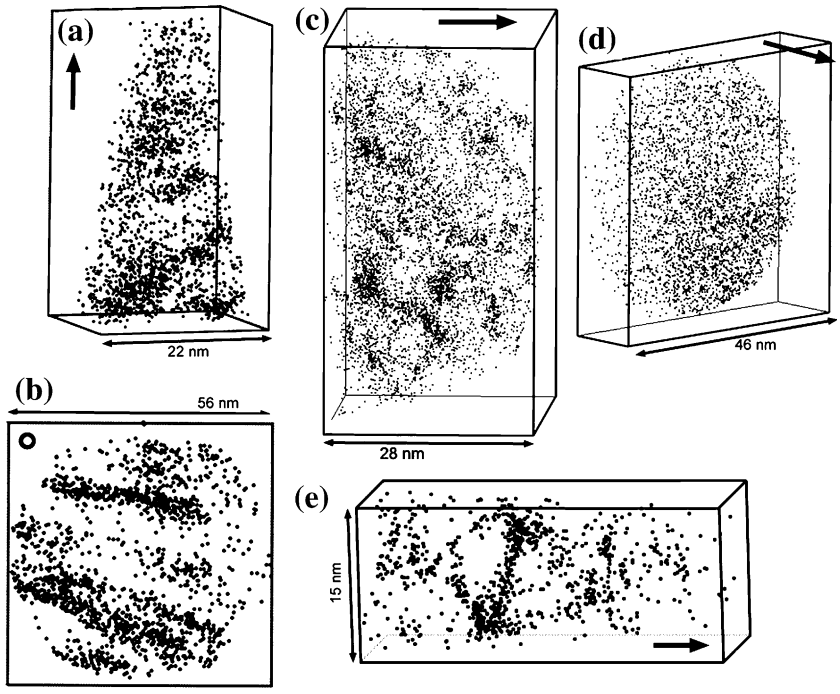

Fig. 5. Three-dimensional reconstruction of Mn distribution in PP Ni–Mn. All atoms other than Mn have been removed from display for clarity purpose. The arrow indicates the tip axis. In (a), it is parallel to the plating direction. In (b)–(f), the tip axis is orthogonal to the plating direction; because of the alignment of the tips, the information on the exact orientation is lost.

periodicity of about 5–10 nm, and Mn concentrations varying between 0 and 0.8 at.% (Figure 5(b)). However, more commonly, APT analyses of in-plane tips exhibit interconnected Mn "clouds" (Figure 5(c) and (d)), with regions free of Mn and regions containing up to 6 at.% Mn. Few analyses exhibit Mn distributions that appear homogeneous (Figure 5(e)).

The DC Ni–Mn deposits have an overall lower Mn concentration. Although the current density is maintained constant, the Mn atoms are clearly not uniformly distributed. Typical reconstructions are shown in Figure 6 where the regions of high Mn concentration are between 30 and 50 nm apart.

No relationship could be established between the Mn distribution and the presence of structural defects such as grain boundaries. For example, Figure 7 shows two slices taken from a three-dimensional reconstruction containing grain boundaries. No Mn enhancement exists at the outlined grain boundaries (black lines).

4. Discussion

4.1. *Role of Mn*

As seen on the cross-section images of Figure 3, any equiaxed grain structure associated with a nucleation layer at the Ni/Cu interface is very thin and all the films exhibit a columnar grain structure. The effect of current density on grain structure complements the trend observed by Buchheit and co-workers, who reported a more pronounced columnar structure with increasing grain size as the current density was increased from 20 to 50 mA cm^{-2} [3]. Although the films used for cross-section observations are thin, the grain structures in the bulk of the blanket films are independent from the texture of the underlying Cu substrate, as confirmed by texture analysis of much thicker films. Therefore, the textures measured at the deposit/solution interface reflect the structure of the films during steady-state growth.

Current density effects with respect to texture of Ni sulfamate is similar to that reported for the texture of Ni Watts deposits. At the lowest current densities, the appearance of fine grain, ⟨110⟩ textured material is typically associated with "inhibited" growth. As current density increases, the growth mode transitions to "uninhibited" or free growth characterized by a coarser grained, predominantly ⟨100⟩ textured microstructure. The principal difference between the DC plated Ni and the DC plated Ni–Mn is that the Mn entirely suppresses the development of the free growth regime at the higher current densities; the net result being that the alloy deposits are fine grain and either predominantly or, at least significantly ⟨110⟩ textured over the entire range of current density examined. The mechanism of how the presence of Mn^{++} ions in the Ni sulfamate electrolyte inhibits the growth of Ni is unclear, although it has been speculated that the incorporation of Mn into Ni films does not result from electrochemical reduction but rather by a surface reaction at the hydrogen-saturated cathode [8, 14]. A further investigation that includes variation in pH may clarify the inhibition mechanism.

In the case of the ⟨110⟩ textured PP Ni–Mn films, most of the plating time is spent at the lower current density, 3 mA cm^{-2}, which leads to the ⟨110⟩ texture in Ni sulfamate. Similar to the DC plated Ni–Mn, the high current density periods in the PP Ni–Mn deposits contribute to the incorporation of Mn without changing the film texture. The grain size is also consistent with the structure observed at low plating current densities.

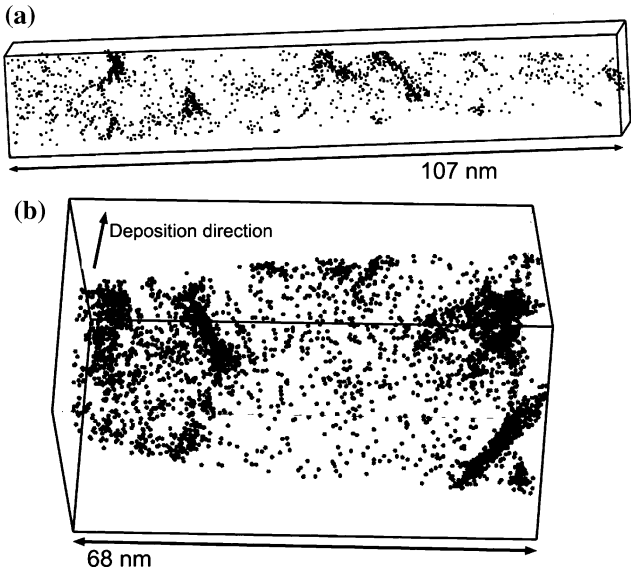

Fig. 6. Three-dimensional reconstruction of Mn distribution in DC plated Ni–Mn. All atoms other than Mn have been removed from display for clarity purpose.

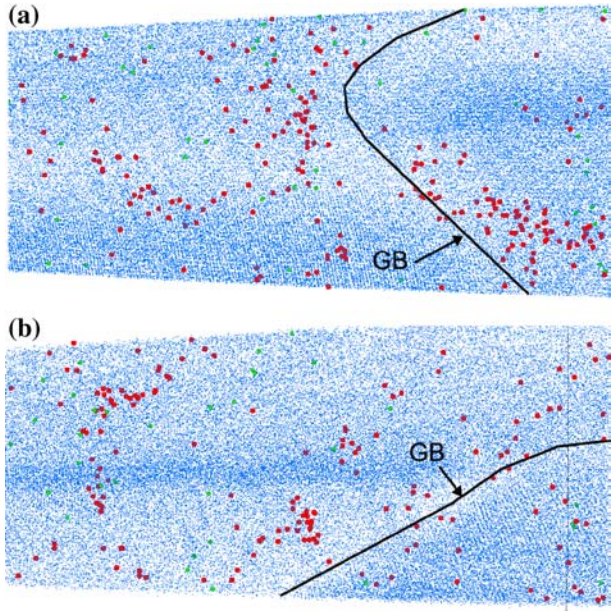

Fig. 7. Slices through a reconstruction containing grain boundaries (black lines) in PP sulfamate Ni–Mn. Ni atoms are blue, Mn atoms are red and oxygen in green. The 3D slices are about $19\times4\times41$ nm^3.

Moreover, the absence of correlation between the position of Mn atoms and grain boundaries does not indicate grain nucleation on Mn-associated impurities.

4.2. *Direct current versus pulse plating*

The more quantitative APT analyses were done to determine if DC and PP Ni–Mn alloys exhibit differences in the Mn distribution. Randomness of the Mn concentration was tested through the distribution of Mn concentration measured in blocks of 1000 atoms. This choice of number of atoms per block, i.e. 1000, is a trade-off between concentration and spatial resolution; the resolution needs to be as large as possible to measure the variations of the small Mn concentration yet still capture the variations over the small characteristic length scales.

Figure 8 presents the expected (based on a random solid solution) and experimentally determined distributions of Mn concentration in solution in both DC and PP plated Ni–Mn deposits derived from the APT analyses. They significantly differ from the expected concentration distributions based on random solid solutions that are indicated by the dashed lines. These random distributions correspond to binomial distributions centered on the overall measured Mn concentrations of the DC and PP Ni–Mn alloys, i.e. 0.17 and 0.45 at.% Mn. The χ^2-statistical test confirms with a 99.9% confidence the non-randomness of the Mn concentration distribution in the as-deposited state. Similar observations of non-uniform compositions have been reported for ED Ni–Fe [15].

In the case of pulse plating, one would expect Mn deposition to be diffusion-limited on the high value of

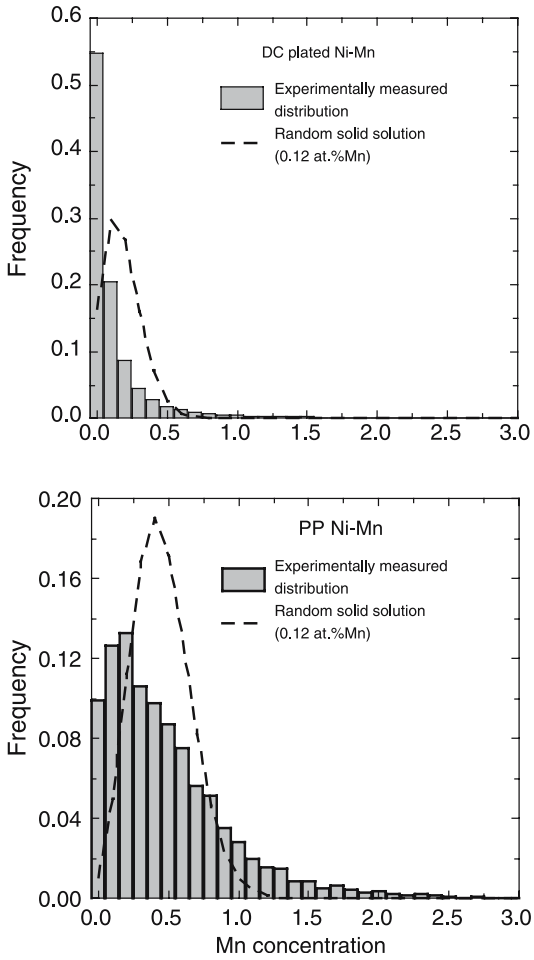

Fig. 8. Mn concentration distributions in DC and PP Ni–Mn compared to predicted distribution in case of random solid-solution (binomial distribution).

the pulse and therefore to deposit uniformly on the surface; while the low value of the pulse would allow for the diffusion of Mn towards the surface. It however does not explain why Mn is also modulated in DC plated films. Although Ni deposition is likely to be kinetically limited because of the deposition parameters, local Mn variations in bath chemistry and compositional oscillations in the bath just above the growing surface may lead to the three-dimensional character of the modulations. The difference between the Mn distribution in DC and PP deposits needs to be investigated further by analyzing in detail the relation between surface topology, species diffusion in the bath, deposition flux and therefore current density. Pulse plating, however, appears to reduce the spatial periodicity of the Mn modulations.

It was originally suggested that pulse-plating would lead to lower stress deposits by a straightforward modulation of the Mn composition, resulting in alternating nanometer scale regions of high-stress (and high-strength) sandwiched by lower stress, soft Ni regions of similar dimensions [2]. The pulse plating conditions used in this study were intended to produce a modulated material consisting, at least in principle, of nanometer

thick, discrete layers of Ni and Ni–Mn, with respective thicknesses of 4.6 and 3.4 nm, according to calculations of the Faraday currents. Parts of the Mn distribution that appear layered have a periodicity that is consistent with the expected value of 8 nm. The APT observations however indicate that the stress relieving mechanism is actually more complex, as pulse-plating appears to smooth out the Mn concentration variations. While the PP Ni–Mn deposits have comparable Mn concentration to DC Ni–Mn deposits that have been plated at high current density, their grain size is finer and their texture is, in detail, different than that of DC Ni–Mn films. These observations suggest that the relieving stress mechanism may be linked to the precise nature of the texture rather than to the spatial distribution of Mn.

5. Conclusions

Current density controls texture and grain structure of Ni deposited from sulfamate baths at 28 °C, pH 3.5 in a similar manner as the Watts Ni deposits plated at higher electrolyte temperature. Average grain size increases and the deposit texture changes from ⟨110⟩ growth to ⟨100⟩ growth as current density increases. $MnCl_2$ addition in the bath modifies the texture of the films by favoring the ⟨110⟩ direction and leads to fine-grained materials at all current densities. The overall Mn concentration scales with current density, but the local Mn concentration varies widely from ~0 up to 6 at.% Mn for both the DC plated and pulse-plated Ni–Mn deposits.

Acknowledgements

Joshua Funamura, Andy Gardea, and Michael Rye are thanked for support in sample preparation and characterization. EAM specially thanks the staff at Imago Scientific Instruments Co., and the Northwestern University Center for Atom Probe Tomography. Sandia is a multiprogram laboratory operated by Sandia Corporation, a Lockheed-Martin Company, for the United States Department of Energy National Nuclear Security Administration under contract DE-AC04-94AL85000.

References

1. R. Weil, H.J. Sumka and G.W. Greene, *J. Electrochem. Soc.* **114** (1967) 449.
2. J.J. Kelly, S.H. Goods and N.Y.C. Yang, *Electrochem. Solid State Lett.* **6** (2003) C88–91.
3. T.E. Buchheit, D.A. LaVan, J.R. Michael, T.R. Christenson and S.D. Leith, *Metall. Mater. Trans. A* **33** (2002) 539–554.
4. S.H. Goods, J.J. Kelly and N.Y.C. Yang, *Microsyst. Technol.* **10** (2004) 498–505.
5. N.V. Mandich and D.W. Baudrand, *Plat. Surf. Finish.* **89** (2002) 68–76.
6. N. Atanassov and V. Mitreva, *Surf. Coat. Technol.* **78** (1996) 144–149.
7. J.W. Dini, *Electrodeposition: The Materials Science of Coatings and Substrates* (Noyes Publications, Westwood, 1993).
8. G.A. Malone, *Plat. Surf. Finish.* **74** (1987) 50–56.
9. A.A. Talin, E.A. Marquis, S.H. Goods and J.J. Kelly, *Acta Mater.* (in press).
10. U.F. Kocks, C.N. Tome and H.R. Wenk, *Texture and Anisotropy, Preferred Orientatoin in Polyscyrtals and their Effect on Materials Properties* (Cambridge University Press, Cambridge, 1998).
11. Information on the BEARTEX package is available via the following web site: http://www.eps.berkeley.edu/~Wenk/TexturePage/beartex.html.
12. J.I. Goldstein *et al.*, *Scanning Electron Microscopy and X-ray Microanalysis* (Kluwer Academic/Plenum Publishing, New York, 2003).
13. M.K. Miller and G.D.W. Smith, *Atom Probe Microanalysis: Principles and Applications to Materials Problems* (MSR, Pittsburg, 1989).
14. N. Atanassov and H.W. Schils, *J. Appl. Electrochem.* **29** (1999) 51.
15. M. Thuvander, M. Abraham, A. Cerezo and G.D.W. Smith, *Mater. Sci. Technol.* **17** (2001) 961–970.